

Multiscale Analysis of Count Data through Topic Alignment

JULIA FUKUYAMA*

Department of Statistics, Indiana University Bloomington, 919 E 10th Street, Bloomington, IN

47408, USA

jfukuyama@indiana.edu

KRIS SANKARAN*

Department of Statistics, University of Wisconsin - Madison, 1300 University Ave, Madison,

WI 53706, USA

ksankaran@wisc.edu

LAURA SYMUL*

Department of Statistics, Stanford University, 390 Jane Stanford Way, Stanford, CA 94305,

USA

lsymul@stanford.edu

SUMMARY

Topic modeling is a popular method used to describe biological count data. With topic models, the user must specify the number of topics K . Since there is no definitive way to choose K and since a true value might not exist, we develop techniques to study the relationships across

*All authors contributed equally to this work and should be included in correspondence.

models with different K . This can show how many topics are consistently present across different models, if a topic is only transiently present, or if a topic splits in two when K increases. This strategy gives more insight into the process generating the data than choosing a single value of K would. We design a visual representation of these cross-model relationships, which we call a *topic alignment*, and present three diagnostics based on it. We show the effectiveness of these tools for interpreting the topics on simulated and real data, and we release an accompanying R package, `alto`.

Key words: topic model; microbiome; community analysis; multiresolution; mixed membership models

Topic models are probabilistic models for dimensionality reduction of count data. They are widely used in modern biostatistics, finding application in population genetics, genome-wide association studies, metabolomics, and microbiome studies [2, 17, 13, 9, 18].

These models are appealing because they are more expressive than clustering yet have simple interpretations [1]. Like clustering, topic models provide a small set of “prototypical” data points; this enables summarization of the overall collection. Unlike clustering, where each sample must belong to exactly one cluster, topic models support varying grades of membership. Therefore, samples are allowed to smoothly blend from one prototype to another. Alternatively, topic models can be viewed as a form of constrained dimensionality reduction, where factors and loadings are constrained to lie on the probability simplex [5]. The sum-to-one constraint can make the results more interpretable than standard PCA, NMF, or factor analysis: each sample can be written as a mixture of underlying types, and each topic is a probability distribution across data dimensions. For example, for microbiome data, each topic can be interpreted as a sub-community of bacteria and each sample is a mixture of a few underlying sub-communities.

Like most clustering and dimensionality reduction methods, topic models come with a hyper-parameter, K , that controls the complexity of the resulting fit, and choosing a good value of K to aid downstream analysis remains a challenge. Past work has focused on automatic selection

of this hyperparameter, typically by referring to the marginal likelihood of a test set [21, 12]. In this study, we explore an alternative, a process we call *topic alignment* (Fig 1, which is based on describing how models fit across a range of K relate to one another.

This reframing has appeared in previous literature, though typically in the context of new models, rather than new algorithms applied to existing models. For example, a hierarchical extension of topic models [3] provides a similar multiscale interpretation of topic structure. However, computational challenges have made these models somewhat difficult to extend and apply, compared to fixed K topic models. In the hierarchical clustering context, a comparison across choices of K is central to the HOPACH algorithm [16], which evaluates cluster stability using a bootstrap procedure.

Instead of introducing a novel multiscale model, we focus on post-estimation comparison of an existing ensemble. This is in the spirit of methodology for comparing clusterings [14, 20], which introduce metrics for navigating the space of clustering results. Similarly, a description of the relationship between models across choices of K is provided by graphical posterior predictive analysis [7, 8]. A posterior predictive check can highlight the lack-of-fit at particular choices of K , in addition to guiding the selection of K . We also note a connection to Tukey’s process of iterative data structuration [19, 10].

Alignment of models across scales naturally supports a coarse-to-fine analysis, ensuring that subtle patterns can be related to their overall context. First, this helps navigate the interpretability-expressivity trade-off associated with different choices of K . Models with small K tend to be more interpretable, but may suppress interesting variation in the data. Conversely, models with large K are more faithful to the data, but can be overwhelming to the analyst. By streamlining comparison across K , we get the best of both worlds — topics at large values of K can be interpreted in context of the coarser ones to which they relate. Second, topic alignment is still relevant to the challenge of choosing K . In a way that is made precise in Section 2.3, true topics tend to be more

stable across choices of K , while spurious ones are more transient. Finally, alignment can help practitioners discover mis-specifications in topic models. For example, it is biologically plausible that microbiome data deviate from the topic model generative mechanism in the following ways,

- Elevated heterogeneity: Topic models assume that all samples are a mixture of a few underlying sub-communities. If samples have more heterogeneity than expected — e.g., due to unmodeled external factors — then topic models may be inappropriate, even for large K .
- Strain switching: There may be strains of a species that compete for the same ecological niche. If one strain is successful, then the other would be expected to be absent. This can result in sharp differences in strains within an otherwise well-defined community structure.

In Section 3, we generate data inspired by these phenomena and apply topic alignment to them. We describe the degree to which the resulting alignments reflect underlying heterogeneity or switching. As long as the mis-specification is not too subtle, topic alignment can suggest specific structure to incorporate into follow-up analysis.

In the remainder of this paper, we present the following contributions,

- The design of algorithms and diagnostics to support the comparison of topic models fit across a range of scales K .
- An analysis of the properties of these algorithms and diagnostics, using simulation experiments across several generative mechanisms.
- An illustration of topic alignment applied to a microbiome data analysis problem.
- The release of an R package, `alto`, implementing these methods.

Sections 1 and 2 review relevant background material and present algorithms and diagnostics for topic alignment, respectively. Subsection 2.4 briefly describes the `alto` package and the

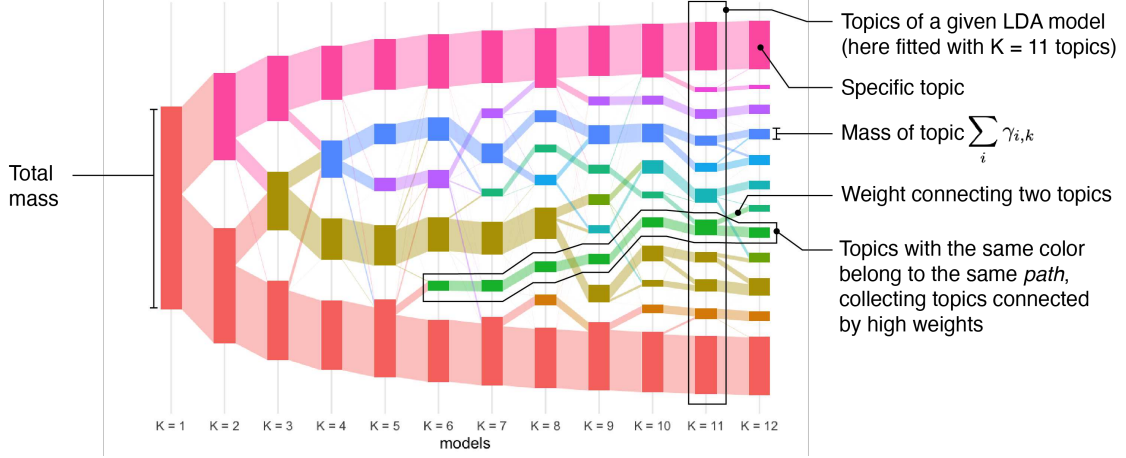


Fig. 1: How to read a topic alignment. Construction of weights is discussed in Section 2.1 and paths are defined in Subsection 2.2.3.

workflow that it supports. Section 3 presents a suite of simulation experiments, with an emphasis on exploring model mis-specification through alignment. Section 4 describes the application of topic alignment to a data analysis problem associated with the vaginal microbiome. This is a setting where high-level structure is dominated by a few well-known species, but where additional, systematic variation is present at finer scale.

1. BACKGROUND

We first review topic models. Then, we summarize approaches to compare probability distributions, which are used in Section 2.

1.1 Latent Dirichlet Allocation

Latent Dirichlet Allocation (LDA) is a flexible way to summarize high-dimensional count data. Suppose that the data are made up of N samples $x_i \in \mathbb{N}^D$. For example, in text analysis, these are the counts of D words across N documents. In the data analysis given in Section 4, these are the counts of D Amplicon Sequence Variants (ASVs)[†] across N samples collected from the study

participants. Let $n_i = \sum_d x_{id}$ be the total count of sample i . Then, LDA supposes that each x_i is drawn independently according to,

$$x_i | \gamma_i \sim \text{Mult}(n_i, B\gamma_i)$$

$$\gamma_i \sim \text{Dir}(\lambda_\gamma \mathbf{1}_K)$$

where the K columns β_k of $B \in \Delta^D$ lie in the D dimensional simplex and are themselves drawn independently from,

$$\beta_k \sim \text{Dir}(\lambda_\beta \mathbf{1}_D).$$

In this mechanism, the $\gamma_i \in \Delta^K$ can be interpreted as mixed-membership weights, with each γ_{ik} giving the degree to which sample i “belongs” to topic K . Since each γ_i can vary continuously through the simplex, the model is more flexible than a simple clustering model, which would assign each sample to exactly one of K clusters (i.e., only corners of the simplex). The three hyperparameters in this model are the number of topics K and the prior parameters $\lambda_\gamma, \lambda_\beta$. Large λ_γ and λ_β result in Dirichlet distributions that place more mass near the uniform distribution. Small λ_γ and λ_β place more mass on edges and corners of the simplex, resulting in sparser γ_i or β_k , respectively.

For example, for microbiome data, each β_k corresponds to a pattern of ASV abundance. Each sample i is a mixture of these underlying communities, with mixing weights γ_i . Note that, though the topics are amenable to compositional interpretations — the β_k lie on the simplex — the original count data are modeled directly, rather than initially transformed to centered-log-ratios, for example. This makes it possible to account for differential uncertainty in samples with high and low sequencing depth and decreasing the amount of processing that takes places between raw data and final interpretation, reducing the risk for analysis errors.

1.2 Simplex Distances and Optimal Transport

We next review methods for comparing probability distributions. These are useful in the LDA context, because the parameters γ_i and β_k all lie on the probability simplex.

We first consider distances on the simplex. Let $p, q \in \Delta^D$ (i.e., two discrete probability distributions over D categories). The Jensen-Shannon Divergence (JSD) between them is defined as

$$JSD(p, q) := \frac{1}{2} \left[\text{KL} \left(p \parallel \frac{1}{2}(p+q) \right) + \text{KL} \left(q \parallel \frac{1}{2}(p+q) \right) \right]$$

where $\text{KL}(a, b) := \sum_i a_i \log \left(\frac{a_i}{b_i} \right)$ is the Kullback-Liebler divergence between a and b . The JSD can be viewed as a symmetrized version of the Kullback-Liebler divergence, allowing it to serve as a distance measure. Intuitively, for p and q to have low JSD to one another, samples from either distribution should have high probability under the averaged distribution $\frac{1}{2}(p+q)$. Alternatively, the cosine similarity cossim $(p, q) := \frac{p^T q}{\|p\|_2 \|q\|_2}$ may be used. The numerator here is large when both p and q place high mass on the same coordinates, and the denominator is smallest when both p and q are far from uniform.

Both the JSD and cosine similarity treat all coordinates of Δ^D symmetrically. They are also only defined when p and q have the same number of categories D . Alternatively, we may relax these constraints, requiring instead only a notion of pairwise similarity between coordinates in p and q . This is formalized in optimal transport, which assigns costs for “transporting mass” between pairs of coordinates. Represent the costs of transporting mass between the D coordinates of p and the D' coordinates of q by a matrix $C \in \mathbb{R}_+^{D \times D'}$. Then, the optimal transport between p and q is the coupling Π minimizing,

$$\begin{aligned} & \min_{\Pi \in \mathcal{U}(p, q)} \langle C, \Pi \rangle \\ & \mathcal{U}(p, q) := \{ \Pi \in \mathbb{R}_+^{D \times D'} : \Pi \mathbf{1}_D = p \text{ and } \Pi^T \mathbf{1}_{D'} = q \}, \end{aligned}$$

where $\langle A, B \rangle$ is shorthand for the Frobenius inner product, $\text{tr}(A^T B)$. The smaller the transport

cost $\langle C, \Pi \rangle$, the more similar the distributions p and q , with respect to the costs induced by C .

A useful analogy is due to Kantorovich [15]. Imagine there are D mines and D' factories. An amount p_i of raw material is produced by mine i ; on the other hand, factory j requires q_j total input. Suppose C captures the transport costs between all pairs of mines i and factories j . Then, the optimal transport plan Π specifies how much material produced by mine i should be shipped to factory j .

2. METHODS

We next set up the problem of topic alignment, provide associated algorithms, and discuss an R package implementation.

2.1 Topic Alignment

Suppose we have estimated topics across an ensemble of LDA models $m \in M$. The topic alignment problem consists of constructing a weighted graph whose nodes are topics from across models and whose edge weights reflect the similarity between the topics. Formally, let $v \in V$ be the set of topics across all models m . We suppose the investigator has specified pairs $e = (v, v') \in E$ of topics that are of interest to compare. Then, an alignment should provide weights $w : E \rightarrow \mathbb{R}_+$ that are large when v and v' have similar estimated parameters, and low otherwise.

The graph $G = (V, E, w)$ contains the result of the topic alignment. Let $k(v)$ denote the topic associated with node v , and suppose it lies in model m . Write $\gamma(v) := (\gamma_{ik(v)}^m) \in \mathbb{R}_+^N$ for the vector of mixed memberships associated with this topic. Similarly, set $\beta(v) := \beta_k^m \in \Delta^D$.

We focus on the case that topics are derived from a sequence of models with increasing K . Then, we can identify each model m with a unique scale k and set $M = \{1, \dots, K\}$. This choice of sequential comparisons makes it possible to perform a multiscale analysis. Topics that, for models with large k , can distinguish between subtle variations in samples, can be related overview topics

from models with small k .

2.2 Algorithms

2.2.1 Weight estimation We propose two methods for estimating weights $w(e)$, which we call product and transport alignment, respectively. In product alignment, we set $w(e) = \gamma(v)^T \gamma(v')$. Intuitively, if two topics have a similar pattern of γ_{ik} 's across samples i , then they are given a high weight (Figure 2a). Further, topics that have small γ_{ik} across all samples are given lower weight, regardless of how similar they may be.

In transport alignment, we compute $w(e)$ by solving a collection of optimal transport problems (Figure 2b). Consider two subsets $V_p, V_q \subset V$; typically, we take these two sets to be all topics v from consecutive models m and $m+1$. Let $p = (\gamma(v)^T \mathbf{1}_N)_{v \in V_p}$ and $q = (\gamma(v)^T \mathbf{1}_N)_{v \in V_q}$. These summarize the “mass” of each topic across all samples, within each of the two sets. Define the cost of transporting mass from node v to v' by $C(v, v') := JSD(\beta(v), \beta(v'))$. This ensures that weights are lower between topics with very different distributions, regardless of sample weights γ_{ik} . Arrange these costs into a matrix of size $|V_p| \times |V_q|$. The weight matrix W between pairs of topics in V_p and V_q is the $\mathbb{R}_+^{|V_p| \times |V_q|}$ matrix formed by solving the transport problem,

$$\begin{aligned} & \min_{W \in \mathcal{U}(p, q)} \langle C, W \rangle \\ & \mathcal{U}(p, q) := \{W \in \mathbb{R}_+^{|V_p| \times |V_q|} : W\mathbf{1}_{|V_q|} = p \text{ and } W^T\mathbf{1}_{|V_p|} = q\}. \end{aligned}$$

We note that in the case that V_p and V_q contain topics from models m and $m+1$, it is natural to construct a directed graph, with edges from topics in model m to those in $m+1$. For a directed graph, it is possible to normalize weights according to either the total inflow or outflow for each node. Specifically, we may normalize weights for edges flowing out of v according to $w_{\text{out}}(v, v') = \frac{w(v, v')}{\sum_{\tilde{v}: v \rightarrow \tilde{v}} w(v, \tilde{v})}$. Similarly, normalization for edges flowing into v is defined by $w_{\text{in}}(v', v) = \frac{w(v', v)}{\sum_{\tilde{v}: \tilde{v} \rightarrow v} w(\tilde{v}, v)}$.

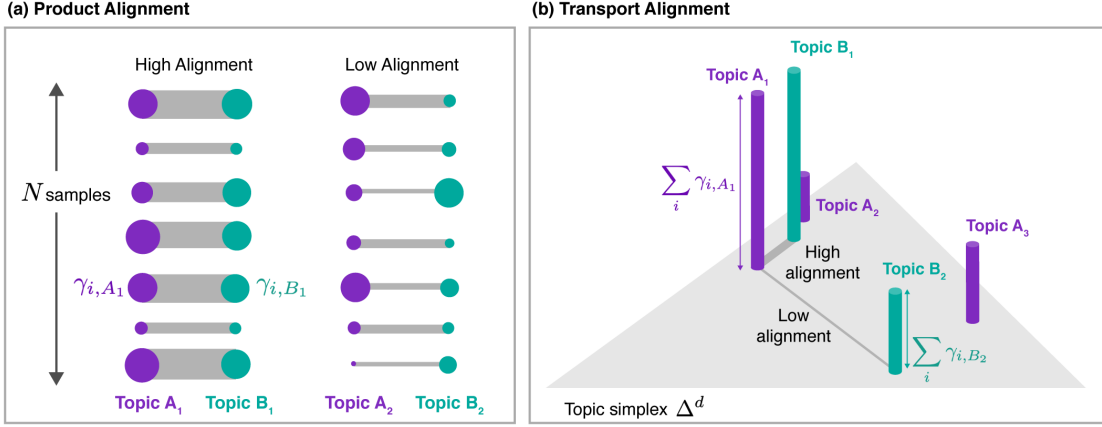


Fig. 2: Each vertical column in (a) corresponds to a topic. Each circle encodes weights γ_{iv} for a single sample i . The width of the links between circles encodes the product $\gamma_{iv}\gamma_{iv'}$. Note that this product is large only if both γ_{iv} and $\gamma_{iv'}$ are large. The product alignment between two topics is high if the sum of products across all N is large. Each vertical bar in (b) describes a single topic v . The heights of bars provide the weights $\sum_i \gamma_{iv}$ for each topic v ; their locations encode $\beta_v \in \Delta^D$. Green and purple topics are estimated by LDA models with $K = 2$ and 3 topics, respectively. In transport alignment, the mass from the green bars is redistributed to the purple bars and alignment weights are derived from the associated optimal transport plan.

2.2.2 Topic ordering Topics are not returned by the LDA fit in a specific order. Consequently, topics connected by high weights across models may have different index k within their respective model. For visualization purposes, it is useful to order topics within each model such that similar topics are close to each other (Figure 3). The ordering procedure seeks the optimal permutation of topic indices $\pi_{1:M}^*$ such that the distance between strongly connected consecutive topics is minimized,

$$\arg \min_{\pi_{1:M} \in \Pi_{1:M}} \sum_{m=1}^{M-1} \sum_{e \in E_{m,m+1}} |\pi_m[k(v)] - \pi_{m+1}[k(v')]| w(e),$$

where the optimization is taken over the set of possible topic permutations Π_m of topic labels in each model m and $E_{m,m+1}$ is the set of edges between topics in models m and $m + 1$. Finally, the reordered topic label for node v at level m is given by $k(v) \leftarrow \pi_m^*(k(v))$.

Instead of searching over all possible permutations, we approximate the optimal solution

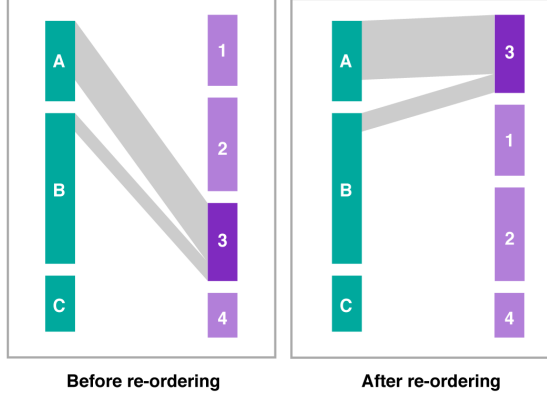


Fig. 3: Given the high alignment weights with topic A, topic 3 index is permuted such that this topic become the first one of its model.

across a sequence of models M by applying a forward and a backward pass, both of which rank the centers of gravity of a topic based on the weights connecting it to topics from the previous (forward pass) or next (backward pass) model. We find that additional forward and backward passes has little impact on the rankings. Specifically, the set of topic indices is updated using Algorithm 1.

```

for  $m = 2:M$  do
     $| k'(v_m) := \text{rank} \left( \sum_{v_{m-1} \in V_{m-1}} k(v_{m-1}) w_{\text{in}}(v_{m-1}, v_m) \right), \forall v_m \in V_m$ 
end
for  $m = M:2$  do
     $| k'(v_{m-1}) := \text{rank} \left( \sum_{v_m \in V_m} k(v_m) w_{\text{out}}(v_{m-1}, v_m) \right), \forall v_{m-1} \in V_{m-1}$ 
end

```

Algorithm 1: Forward and backward pass for the topic ordering algorithm. In the forward pass, topics are indexed so that they are close to the source topics from which they draw the most weight, while in the backward pass, they are placed near their high weight descendants.

2.2.3 Paths Topic reordering places topics with high alignment weights next to one another, giving the appearance of chains of mutually similar topics. To highlight this phenomenon, we partition the alignment graph into a collection of paths. The partition is grown iteratively, adding topics to existing subsets based on alignment weights.

Let $\text{Path}(v)$ be the path ID associated with topic v . For each topic $v \in V_M$, we initialize

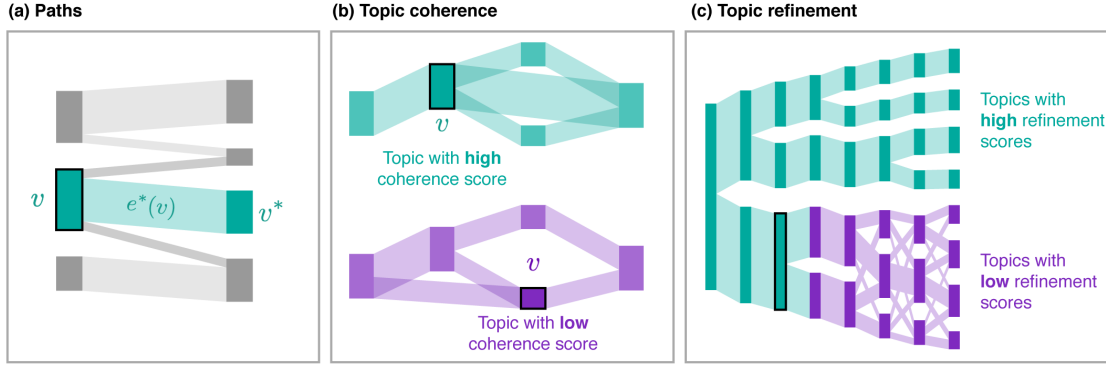


Fig. 4: (a) To assign a path to a topic v , the edges $e^*(v)$ from which topics v derive most of their weight are identified. (b) A topic has a high coherence score if all normalized weights (w_{in} and w_{out}) between this topic and topics on the same path are large. (c) A topic has a high refinement score if the downstream alignment structure is “tree-like”, i.e. if all descendant topics recognize v as their main parent. Note that a topic v (highlighted by a black outline here) may have a low coherence score but a high refinement score.

$\text{Path}(v) = k(v)$. Suppose $\text{Path}(v)$ is known for all $v \in V_{m+1}$. Then, the path membership $\text{Path}(v)$ of a node $v \in V_m$ is set to $\text{Path}(v^*)$, where

$$v^* := \arg \max_{v' \in V_{(m+1):M}} w_{\text{out}}(v, v') + w_{\text{in}}(v, v'),$$

is the topic from one of the levels $m+1, \dots, M$ that shares the highest total normalized weight with v .

2.3 Diagnostics

We next propose three diagnostic measures that compactly describe the results of a topic alignment. These statistics reflect the added value of introducing each additional topic, the specificity of ancestor-descendant ties, and the coherence of topics across K . In addition to summarizing the alignment, these statistics can also serve to diagnose model mis-specification in the original fits.

2.3.1 Number of paths If a collection of models with large K nonetheless places most mass on a small subset of topics, then a more parsimonious model with only these topics may be sufficient. This diagnostic counts the number of *paths* found by the iteration of Subsection 2.2.3, excluding those used at initialization. Formally, this is the size of the set $\cup_{m=1}^{K-1}\{\text{Path}(v) : v \in m\}$

In simulations below, we find that, when a topic model is appropriate, the true value K is captured by a plateau in the number of paths. Hence, this metric can be used analogously to the identification of an “elbow” from a scree plot. Further, consistently slow growth in the number of paths identified may indicate departures from the assumed LDA model. Examples of both phenomena are provided in Section 3. The number of paths is a property of a model within the alignment. In contrast, the scores introduced below focus on individual topics.

2.3.2 Topic Coherence We call a topic *coherent* if it is found in models fitted across a range of values of K . When coherent topics are recovered across multiple levels of an alignment, there is more evidence that the discovered structure is real, because it is not sensitive to the particular K of the model used.

Topic coherence is defined in the context of paths. It measures the similarity between a given topic v and the other topics on the same path $\text{Path}(v)$. It is defined as,

$$c(v) = \frac{1}{|\text{Path}(v)|} \sum_{\{v' : \text{Path}(v') = \text{Path}(v)\}} \min(w_{\text{in}}(v, v'), w_{\text{out}}(v, v')).$$

Our simulations illustrate how this score can be used to identify “good” values of K in LDA as well as detect departures from assumed LDA structure. Note that coherence focuses solely on the path containing a topic. We introduce another measure, topic refinement, to reflect the richer branching pattern downstream of a topic.

2.3.3 Topic Refinement A topic identified at a small value of K may have low coherence but still be a useful topic if it is the sole ancestor of topics in subsequent models. We expect true

topics and compromises between true topics to have this property. We introduce the *refinement* score to identify such topics.

Recall that for a node v' , $w_{\text{in}}(v, v')$ measures the extent to which mass at v' flows from parent node v . For each v , the refinement score is a weighted average of $w_{\text{in}}(v, v')$ over all its children v' . More formally, collect topics into levels V_1, \dots, V_L . We define the refinement score of node v in level l as

$$r(v) = \frac{1}{L-l} \sum_{l'=l+1}^L \sum_{v' \in V_{l'}} w_{\text{out}}(v, v') w_{\text{in}}(v, v'). \quad (2.1)$$

To better understand this score, we can establish its properties in some simple cases (proofs given in the supplementary materials). Continuing to assume that node v is in level l , we have

- $r(v) = 1$ if and only if $w(v, v'_l) > 0$ implies $w(u, v'_l) = 0$ for any $u \in V_l \setminus \{v\}$. This condition means that every descendant of v has v as its sole parent in level l .
- Suppose that for every $v' \in V_{l'}$, we have fixed weights $w(v, v')$. Then $r(v) \rightarrow 0$ when for each w s.t. $w(v, v') > 0$, $w(u, v') \rightarrow \infty$ for some $u \in V_l \setminus \{v\}$. That is, $r(v)$ will be minimized if all of the descendants of v descend primarily from other nodes in level l .
- If all the weights in the graph are equal, we will have $r(v) = 1/|V_l|$.

These results have the following interpretations. The score is maximized if a node's descendants descend solely from it, as we expect to see for nodes corresponding to true topics or mixtures of true topics. The score is smaller, $\frac{1}{|V_l|}$, if all the edge weights are equal and there is no relationship between the topics estimated at the different levels. The score is smallest for nodes that don't have any descendants that recognize them as parents at all.

2.4 R package

We have released an R package, `alto`, to support *alignment* of *topics* from LDA models. The package provides functions for

- Fitting a set of topic models.
- Aligning topics across a collection of models, identifying paths, and computing coherence and refinement measures from the alignment.
- Visualizing the resulting alignment object.

The design emphasizes the modularity of the alignment workflow, and separate functions are given for each of the steps above. To illustrate, we include an example use of the package on random multinomial data.

```
library(purrr)
library(alto)

# simulate data and fit models
x <- rmultinom(20, 5000, rep(0.1, 500))
lda_params <- setNames(map(1:10, ~ list(k = .)), 1:10)
lda_models <- run_lda_models(x, lda_params)

# perform alignment and plot
result <- align_topics(lda_models)
plot(result)
```

Note that `result` is an S4 class (class `alignment`) with its own plot method. This class is associated with accessor functions, for extracting the underlying model parameters (`models()`), alignment weights (`weights()`), and topic-level diagnostics (`topics()`).

In addition to the product and transport methods that are currently implemented, the package allows users to pass in arbitrary functions for computing weights between sets of topics. Further, in addition to computing alignments across a sequence of increasing K , the package

implements topics comparison and weight construction over arbitrary topic graphs. Examples of these functions, as well as all data analysis and simulations described here, are available as package vignettes. The package homepage is available at lasy.github.io/alto/ and its source code can be found at github.com/lasy/alto.

3. SIMULATIONS

We next study the extent to which learned topic alignments and their associated diagnostics distinguish between types of variation that can arise in count data. We apply methods in a few controlled settings, verifying that derived interpretations are consistent with the known generative mechanism. We investigate alignment when simulating from true LDA models as well as under certain types of mis-specification. The latter cases inform the extent to which alignment can inform model assessment.

3.1 *Latent Dirichlet Allocation*

If the data were in fact simulated from an LDA model with K topics, then what will the associated topic alignment and diagnostics look like?

We simulate $N = 250$ samples $x_i \in \mathbb{N}^D$ from an LDA model with true $K = 5$ true topics. For mixed memberships, we draw $\gamma_i \sim \text{Dir}(0.5\mathbf{1}_K)$, while topics are assumed sparser, with $\beta_k \sim \text{Dir}(0.1\mathbf{1}_D)$. These parameters have been chosen to maintain simplicity while exhibiting both high-dimensionality in x_i and sparse structure in γ_i and β_k . At this scale, alignments can be made interactively. To fit LDA models with $K \in \{2, \dots, 10\}$ requires 352 seconds[†]. Computation of product and transport alignments each takes 5 - 6 seconds.

With this setup, we simulate 200 datasets and fit models with $K \in \{2, \dots, 10\}$ topics. Each set of models is aligned using both the product and transport methods. The product and transport alignments from a randomly chosen replicate are shown in Figure 5. The primary distinguishing

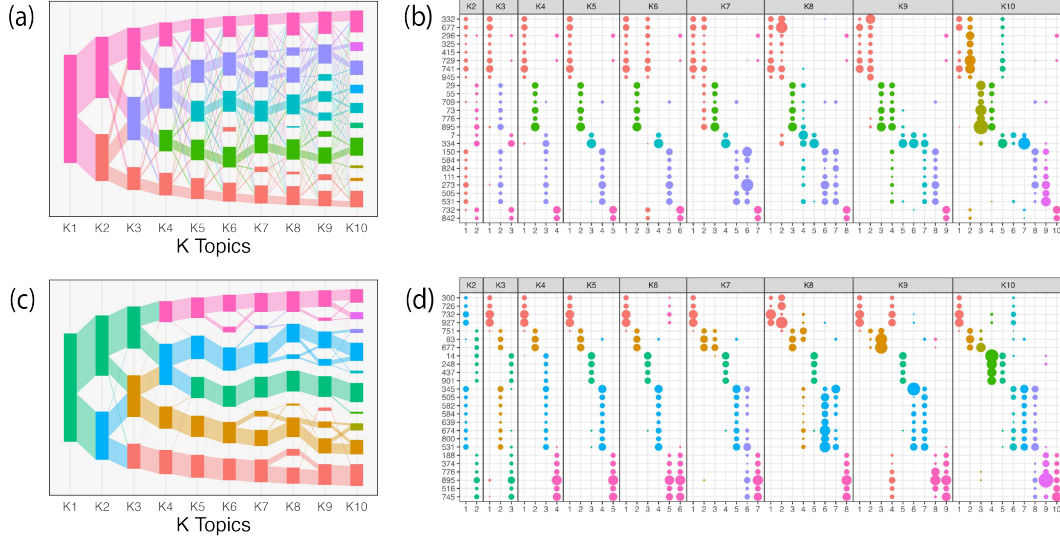


Fig. 5: Alignments for data simulated from LDA with $K = 5$. Parts (a) and (c) are estimated using product and transport alignment, respectively. Rectangles correspond to topics, and their sizes give the mass $\sum_i \gamma_{ik}$. Vertical sections give fitted models. The width of links encodes the weights $w(e)$. Topics and edges are colored to show paths. Parts (b) and (d) give β_{kd} , colored in according to (a) and (c), respectively. Each column encodes a topic, each row is a dimension, and circle size is proportional to β_{kd} . Sets of topics from one model are grouped into panels. Circles with $\beta_{kd} < 0.001$ are omitted. Dimensions d are sorted according to Distinctiveness (d) := $\min_{l \neq k} \beta_{kd} \log \frac{\beta_{kd}}{\beta_{ld}} + \beta_{ld} - \beta_{kd}$, as in [6], but with k, l varying over topics from multiple models. Only the 25 most distinctive dimensions are displayed.

feature between product and transport alignments is the sparsity in weights estimated using the transport approach. Both alignments provide hints that $K = 5$,

- The number of paths (i.e. number of distinct colors) remains 5 for $K > 5$.
- For $K \leq 5$, most mass is conserved along a few major paths. For $K > 5$, this structure fragments and each topic tends to align with multiple descendant topics.

Next, consider diagnostics across all simulation replicates. Figure 6 counts the number of paths at each K . Up to $K = 5$, and for most simulation runs, each new topic created a new path. For $K = 2, 3$, product alignment tended to underestimate the number of true topics more frequently

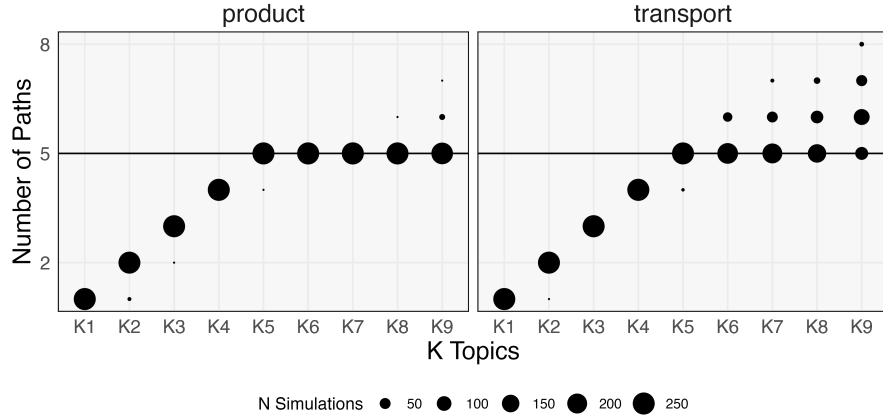


Fig. 6: The number of estimated paths across simulation runs from a true LDA model with $K = 5$. The size of each circle describes the number of replicates for which that number of paths was identified. The estimates level off at the true value $K = 5$. The product method tends to be more conservative, and is less prone to overestimate the number of topics, compared to the transport method.

than transport alignment. For $K = 5, 6$, all alignments estimated that 5 paths were present, and for larger K , additional topics were sometimes added to this subset. Transport alignment tended to more frequently overestimate the number of paths. For example, transport alignment occasionally found up to 8 paths when $K = 9$, while product alignment rarely estimated more than 5 topics.

Figure 7 shows topic-wise refinement scores as a function of K in the alignment[§]. The distribution of refinement scores show an abrupt drop-off for $K > 5$ for both alignment as topics with low similarity with the true topics have low refinement scores. For $K < 5$, refinement scores remain high as topics in these models are parents of true topics.

Overall, two practical rules of thumb are (1) a rapid drop-off in refinement scores indicates low-dimensional structure and (2) topics with high refinement scores are more likely to reflect true topic structure.

These simulations are a sanity check — in the case that data are exactly generated by an

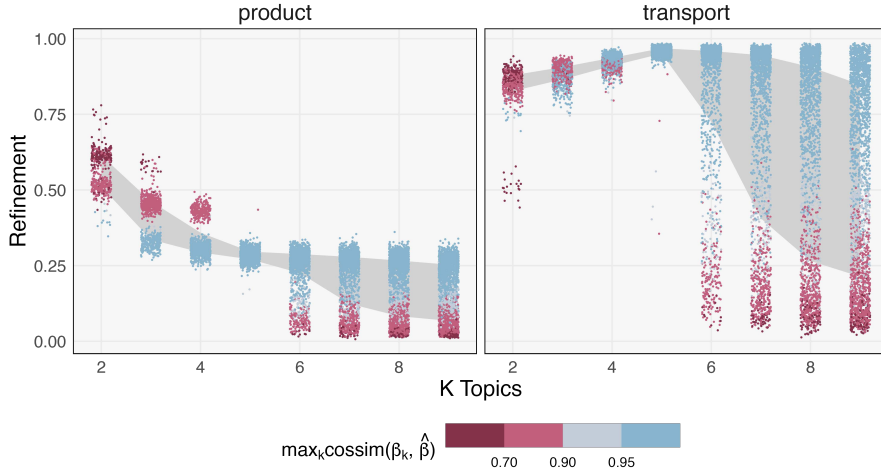


Fig. 7: The distribution of refinement scores across simulation runs from an LDA model with $K = 5$ true topics. The first and third quartiles of refinement at each K are marked by a grey envelope. Estimated topics $\hat{\beta}$ are shaded in according to $\max_{k \in \{1, \dots, 5\}} \text{cossim}(\hat{\beta}, \beta_k)$, the maximum cosine similarity to any of the 5 true topics. In practice, these cosine similarities would be unknown. A drop-off in refinement scores is noticeable for a subset of topics beginning at $K = 6$, suggesting that this diagnostic is sensitive to the introduction of unnecessary topics.

LDA model with a known K , then alignment can help identify it. However, a number of methods are available for selecting K when models are correctly specified, and real data are unlikely to so perfectly correspond to a proposed generative mechanism. In the spirit of “all models are wrong, but some are useful,” we consider scenarios where an LDA model is fit to data that are not simulated from the LDA mechanism, but where alignment can nonetheless inform an understanding of the essential latent structure.

3.2 LDA with background variation

To begin describing properties of alignment in this approximate regime, we simulate data from the case where sample compositions exhibit an extra level of heterogeneity not present in LDA. We suppose that most, but not all, variation in latent sample compositions lies on a K -dimensional subspace spanned by K topics B . The closer the compositions lie to this subspace, the closer the

LDA model is to being correct. Specifically, we simulate from,

$$\begin{aligned} x_i | B, \gamma_i, \nu_i &\sim \text{Mult}(x_i; N_i, \alpha B \gamma_i + (1 - \alpha) \nu_i) \\ \nu_i &\sim \text{Dir}(\lambda_\nu) \\ \gamma_i &\sim \text{Dir}(\lambda_\gamma) \\ \beta_k &\sim \text{Dir}(\lambda_\beta). \end{aligned}$$

This generative mechanism is identical to that of LDA, except that instead of being centered around $B\gamma_i$, sample i is centered around $\alpha B\gamma_i + (1 - \alpha) \nu_i$ for a $\nu_i \in \Delta^D$ drawn without reference to the K topics in B .

As before, we simulate with $N = 250, D = 1000, K = 5$. For each $\alpha \in \{0, 0.05, \dots, 1\}$, we generate 50 datasets and then fit and align topic models with $K \in \{1, \dots, 10\}$. Randomly chosen alignments for a range of α are given in Supplementary Figure 1. For large α , most mass is concentrated in 5 core paths, and there is limited exchange from one topic to another. For small α , mass is more evenly distributed across branches and a high-degree of exchange is present.

The number of paths across K for each α is shown Figure 8. The panels on the right match Figure 6, with a quick increase in the number of paths for $K \leq 5$, and an only gradual increase afterwards. In contrast, the $\alpha = 0$ panel shows that the number of paths increases more gradually as a function of K , and that, across simulation replicates, there is more variation in the number of paths. The definition of paths appears effective at distinguishing low from high-rank sample compositions — a gradual increase in the number of paths, without any visible plateau, would suggest that an LDA model is missing true sample-to-sample variation, even with large choices of K .

The coherence of all estimated topics is shown in Figure 9. Each panel is read like Figure 7, but where the y -axis is coherence. For large α , the upper envelope of coherence scores rapidly increases up to $K = 5$. For $K > 5$, the lower envelope rapidly drops off while the upper envelope

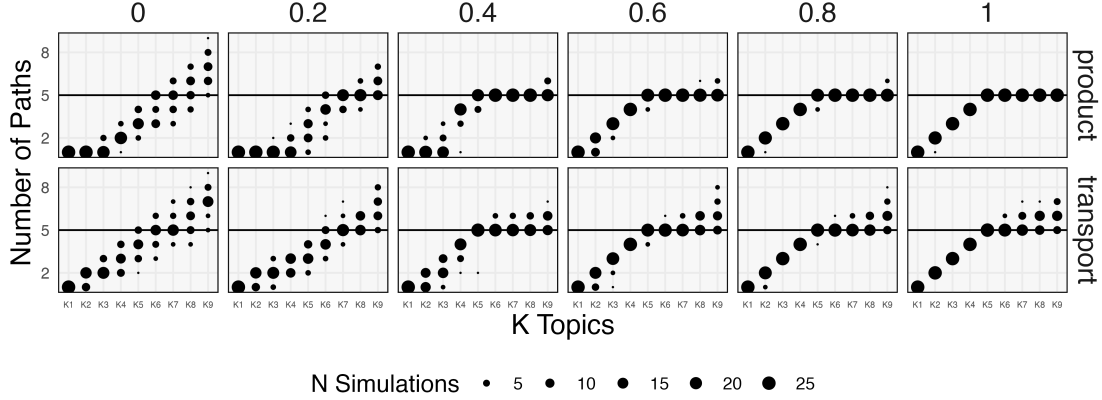


Fig. 8: The estimated number of paths varies as a function of α . Each panel corresponds to one α and each circle gives the number of simulation replicates. The closer the data are to being drawn from an LDA model, the faster the initial increase in the number of estimated paths and the more definitive the plateau at $K = 5$.

slightly decays. This display suggests that, when an underlying LDA model is more approximately correct, the associated alignment includes more coherent topics with a peak coherence around the true latent dimensionality.

Figure 10 shows the analogous display for refinement. In the small α case, at any given K , all topics have essentially the same refinement score, and the score is the one we would expect in the situation where there is no relationship among the topics at different levels. In contrast, in the more approximately low rank, large α case, a larger spread in scores is visible. As before, the topics with the highest refinement scores following $K \geq 5$ have high cosine similarity with the true topics, and the $K = 5$ transition is marked by an increase in the spread of refinement scores and a leveling off of the upper envelope. Further, reading each panel from left to right, we find that the upper envelope of refinement scores gradually increases to 1.

Altogether, these diagnostics suggest that alignment can detect departures from the underlying topic model assumption that samples are concentrated on a K -dimensional topic simplex, across a range of candidate K . Paths with low coherence can be a warning flag. Further, low

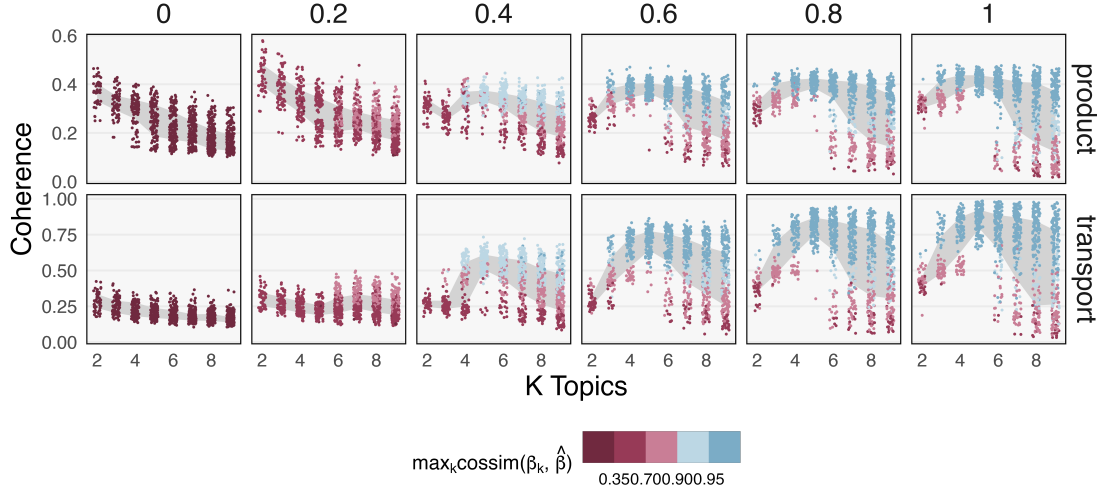


Fig. 9: Topic-wise coherence when background variation is present. Simulation runs across α are arranged across columns, and rows give the alignment method used. For small α , coherence drops-off starting at $K = 1$, with no visible increases. For larger α , a subset of topics has elevated coherence and the largest average topic coherence occurs at the true latent dimensionality.

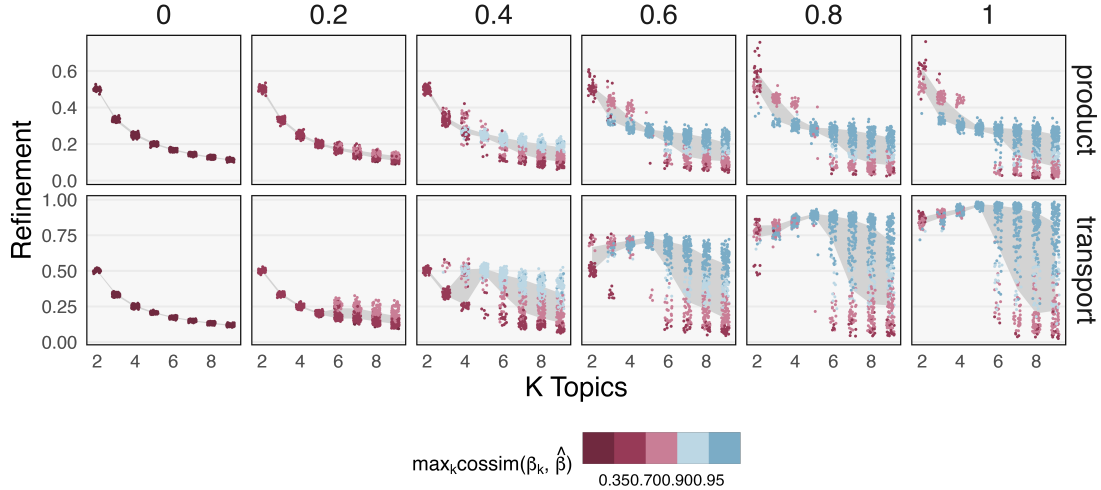


Fig. 10: Refinement scores are higher and exhibit larger range when the LDA model is approximately correct. Each point gives the refinement score of one topic across simulation replicates at a given level K . The range and trend refinement scores can be used to distinguish between datasets that have more or less unmodeled heterogeneity.

refinement scores and the absence of any plateau in the number of paths may suggest that observations exhibit higher sample-to-sample variation than an LDA model alone may capture.

Since it is possible to simulate new data from each fitted LDA model, these guidelines can be formalized into a graphical posterior predictive check. Posterior predictive samples can be drawn from the model with the largest K , which has the most flexibility. Aligning topic models fit to these data could provide a reference distribution for each of the diagnostics, and comparing the observed measures with this reference can give evidence for or against model fit.

3.3 Strain switching

Our final simulation studies whether alignment can detect mis-specifications in topic modeling due to highly correlated topics. Our setup is motivated strain switching in some microbiome environments [11]. In this situation, there are strains that can be exchanged between what are otherwise similar communities. These strains can be thought of as being functionally equivalent, competing for a niche within an ecosystem. The consequence is that two nearly identical communities may be present in the ecosystem, but with systematic differences for some strains. From a topic modeling perspective, these communities have anti-correlated topic memberships – only one of the competing strains can be present in a sample at a time.

The existence of these communities can be detected by comparing topics estimated at different scales. At coarse scale, two communities may be indistinguishable from one another, swamped by larger variations in species signatures across the ecosystem. At finer scale, the subsets of strains that distinguish them may become apparent after close inspection of the estimated topics.

Our goal is to study the extent to which alignment can support this multiscale analysis. Our simulation mechanism first draws γ_i and β_k as in the simulations above. Instead of directly using β_k , however, perturbed versions $\tilde{\beta}_k^r$ are generated for $r \leq R_k$, a pre-specified number of perturbed replicates R_k . The perturbation mechanism is given in Supplementary Algorithm 1. The resulting

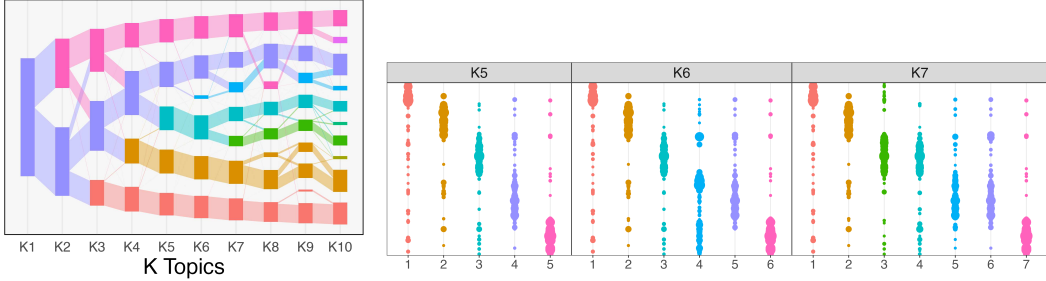


Fig. 11: An alignment from one replicate of the strain switching simulation with $S = 230$. Only the 200 most distinctive dimensions are displayed. The purple-dark blue and green-light blue pairs of branches correspond to two perturbed versions of the same underlying community, as suggested by the similar columns of β_{kd} for $K = 6, 7$ and confirmed by the similarity analysis in Figure 12.

$\tilde{\beta}_k^r$ and $\tilde{\beta}_k^{r'}$ differ only on a subset of S coordinates and can be viewed as functionally equivalent sub-communities. Given perturbed topics, sample i is drawn by first randomly selecting one perturbed version from each of the K topics,

$$\beta_k^i \sim \text{Unif} \left(\left\{ \tilde{\beta}_k^1, \dots, \tilde{\beta}_k^{R_k} \right\} \right)$$

binding the results into a K column matrix B_i , and then drawing,

$$x_i \sim \text{Mult}(n_i, B_i \gamma_i)$$

as in standard LDA.

We set $K = 5$ and $(R_1, \dots, R_5) = (2, 2, 1, 1, 1)$. We draw $N = 250$ samples with dimension $D = 1000$. We use $S = 230$; results with varying S are given in the supplement. In the microbiome interpretation, our samples include counts of 1000 species each, and 5 underlying community types are present. Two versions of the first two types are present, differing on a subset of S competing species.

The resulting alignment is given in Figure 11. The learned topics for $K = 5$ to 7 are given in the right panel. We note that, at $K = 6$, the purple and dark blue topics have similar weights across many, but not all species. Likewise, at $K = 7$, the light blue and green topic signatures

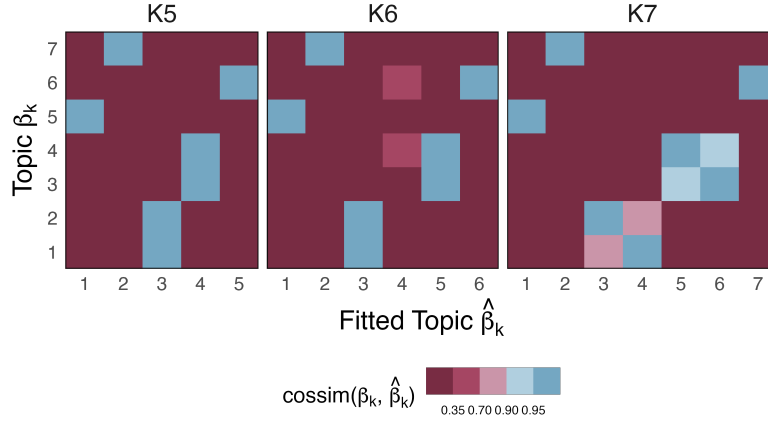


Fig. 12: Cosine similarities between known and estimated topics across increasingly finer-scale models m . Rows 1-2 and 3-4 corresponding to perturbed versions of two underlying communities. For $K = 5$, the estimated topics do not distinguish between versions. At $K = 6$, rows 3 and 4 are slightly distinguished from one another, and at $K = 7$, both sets of perturbed topics are detected.

are similar. The accompanying flow diagram shows that, in both cases, the pairs of similar topics had been merged when $K = 5$, suggesting that the model begins to detect perturbed versions of the same topics once K is increased.

To attribute these differences to the known perturbation mechanism, we compute the cosine similarity between estimated and true topics. Figure 12 shows the cosine similarity $\xi_{kk'}^m := \text{cossim}(\beta_k, \hat{\beta}_{k'}^m)$ for models m with 5 to 7 topics. Each row corresponds to a true topic; rows 1-2 and 3-4 are perturbed versions of two underlying sub-communities, respectively. For $K = 5$, the patterns of cosine similarities across rows 1-2 and 3-4 are similar, suggesting that the estimated topics are not sensitive to strain switching. However, for $K = 6$ and 7, new topics emerge that distinguish between the pairs of nearly equivalent sub-communities. The off-diagonal elements for the two squares indicate that the newly estimated topics remain similar to both versions of the underlying mechanism. However, since only a subset of species is perturbed in each version, some remaining similarity is to be expected.

4. DATA ANALYSIS

We applied topic alignment to vaginal microbiome composition data; the results are given in Figure 13. The data are ASV counts from longitudinal samples collected throughout pregnancy in 135 individuals [4]. In most individuals, the vaginal microbiota present a low heterogeneity compared to other human microbiomes: one of four Lactobacillus species (*crispatus*, *iners*, *gasseri* or *jensenii*) completely dominates the flora. However, some individuals may present “dysbiosis,” defined as the absence of Lactobacillus dominance and the presence a high compositional diversity. Historically, vaginal microbiota data have been clustered into five community state types (CST), four of them corresponding to one of the four Lactobacillus, and the fifth one being “everything else.” Clustering methods having not been very successful at identifying sub-types in this fifth CST. Topic analysis thus offers an opportunity to identify communities that may co-exist.

Applying topic alignment to these data, we observe that the number of paths (Figure 13a) shows a small plateau around $K = 12$ with both methods (product and transport). As in the simulations, the number of paths are lower and the plateau is stronger when paths are identified by the product rather than by the transport alignment. The fact that the plateau is small is likely indicative that the data generation process does not strictly follow the LDA model assumption. However, most of the identified topics around $K = 12$ are coherent across K (Figure 13b). Among these twelve topics, we find four topics associated with each of the dominant Lactobacillus species.

Further investigating the alignment and parent models provides interesting insights on the remaining non-Lactobacillus topics. First, we observe that the four Lactobacillus topics are already present at $K = 7$. In that model, the three remaining topics are non-Lactobacillus topics. Among these, one topic, dominated by a specific strain of Gardnerella and Atopobium, remains coherent across models (Figure 13b-d). The two remaining topics at $K = 7$ have little overlap and high refinement scores (Figure 13c), suggesting that these topics successfully identify two distinct groups of sub-communities.

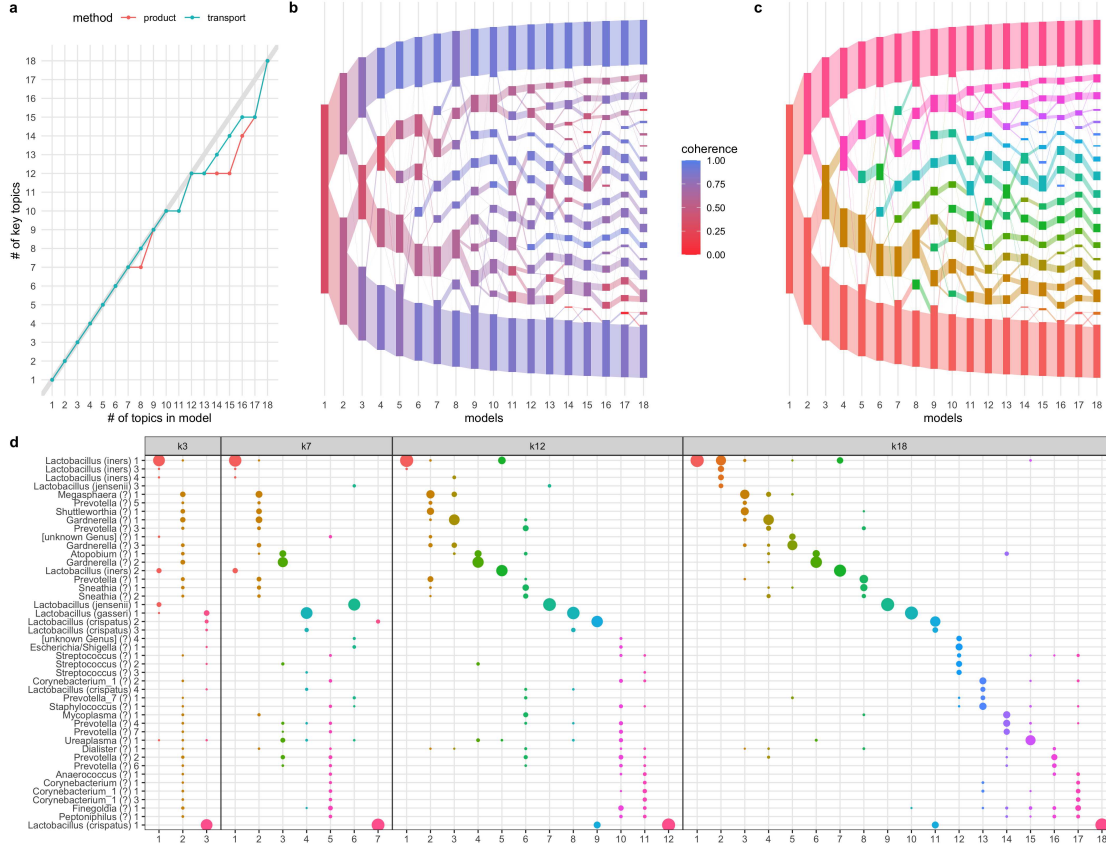


Fig. 13: (a) Number of paths for each number of estimated topics in the LDA model. Number of paths identified by the transport method are shown in blue, those identified by the product method are shown in red. (b-c) Transport alignment of topics across K where topics are colored by their coherence (b) or by paths (c). (d) Topic composition (dot size shows estimated β) for $K \in 3, 7, 12, 18$. Topics (x -axis) are colored by path (see panel b). Species (y -axis) are ordered by the topic with the highest β for that species in model $K = 18$.

By $K = 18$ topics are sparse and share little overlap (Figure 13d), which may reflect overfitting.

5. DISCUSSION

We have introduced techniques for aligning topics from across an ensemble of topic models. The resulting estimates provide a multiscale view of count data, showing how topics from large and

small K models compare and contrast with one another. We frame the alignment problem as the construction of the appropriate weighted graph whose nodes represent topics and whose edges encode topic similarity. We provide algorithms for estimating weights based on either the inner product or the optimal transport between fitted model parameters. Based on these alignment weights, we proposed diagnostics describing (1) the extent to which any given topic persists across a range of K (coherence score) and (2) the definitiveness with which finely-resolved topics emerge from coarser ones (refinement score). We studied the properties of the proposed methods through a series of simulations, emphasizing the potential for alignment to detect biologically plausible departures from the LDA generative mechanism. We also applied the overall workflow to a vaginal microbiome dataset and recovered both known, high-level CSTs, and novel finer-grained sub-community structure.

We note several limitations and opportunities for future study. We have not provided any theoretical guarantees about the estimated alignment weights or diagnostics. In order to make our approach applicable to the ensembles of fitted LDA models that are most frequent in practice, we have deliberately avoided proposing an overarching multiscale model. Requiring a new model would increase the burden for adoption – it is easier to compute post-estimation statistics within a familiar workflow. Nonetheless, though beyond our scope, it would be worthwhile to understand the behavior of alignment weights or diagnostics in such a multiscale setting where model parameters are assumed to be drawn from a plausible distribution.

Further, we have not incorporated any interactive visualization principles to streamline the analysis of the final alignment data structure. The static views provided by our package describe a single aspect of alignment at a time, showing the alignment weights, the estimated model parameters, and diagnostics in isolation from one another. It would be useful to link these views interactively. For example, the “top” species associated along each branch could be highlighted interactively, or the species whose distributions change the most from one topic to the next.

Also absent from our views are any visualizations of how individual samples relate to the topic alignment overall.

Finally, we note that, though we have focused on the case of increasing K , the principle of computing summaries that characterize an ensemble of models is more generally applicable. For example, the choice of hyperparameters $\lambda_\gamma, \lambda_\beta$ controls the sparsity of the posterior mixed membership and topic estimates. A view of which estimates are most strongly influenced by these hyperparameters would be informative. Further, in the data integration context, it may be simpler to relate separate models fit across data modalities rather than to construct a new global model for each new combination of component modalities. Similarly, for datasets collected across multiple sites or environments, alignment may provide a compromise between fitting a separate model per site, which fails to pool any shared information, and implementing a full hierarchical model, which can be a labor-intensive exercise.

As the types of data incorporated in biostatistical studies grow in number and complexity, flexible techniques for dimensionality reduction and visualization will continue to be an important component of the data analysis workflow. Exploratory analysis can guide the critical examination of complex problems, and topic alignment is a simple but useful addition to the toolbox available for count data.

6. SOFTWARE

The R package `alto` is available at lasy.github.io/alto. Simulations and data analysis can be reproduced through package vignettes. Scripts for reproducing simulations in a high-performance computing environment are available at github.com/krisrs1128/topic_align.

7. SUPPLEMENTARY MATERIAL

Supplementary figures, algorithms, and proofs are available online at <http://biostatistics.oxfordjournals.org>.

ACKNOWLEDGMENTS

The authors thank Susan Holmes and xxxx for fruitful discussions and constructive feedback on the manuscript. *Conflict of Interest:* None declared.

FUNDING

LS was supported by the Bill and Melinda Gates Foundation grant OPP1189205-2019 awarded to J. Ravel (Principal Investigator, University of Maryland) and D. Relman (Project Director, Stanford University).

REFERENCES

Edoardo M Airoldi, David M Blei, Elena A Erosheva, and Stephen E Fienberg. Introduction to mixed membership models and methods. *Handbook of mixed membership models and their applications*, 100:3–14, 2014.

Hussein Al-Asadi, Kushal K Dey, John Novembre, and Matthew Stephens. Inference and visualization of dna damage patterns using a grade of membership model. *Bioinformatics*, 35(8):1292–1298, 2019.

David M Blei, Thomas L Griffiths, Michael I Jordan, Joshua B Tenenbaum, et al. Hierarchical topic models and the nested chinese restaurant process. In *NIPS*, volume 16, 2003.

Benjamin J. Callahan, Daniel B. DiGiulio, Daniela S. Aliaga Goltzman, Christine L. Sun, Elizabeth K. Costello, Pratheepa Jeganathan, Joseph R. Biggio, Ronald J. Wong, Maurice L. Druzin,

Gary M. Shaw, David K. Stevenson, Susan P. Holmes, and David A. Relman. Replication and refinement of a vaginal microbial signature of preterm birth in two racially distinct cohorts of US women. *Proceedings of the National Academy of Sciences*, 114(37):9966–9971, September 2017.

Peter Carbonetto, Abhishek Sarkar, Zihao Wang, and Matthew Stephens. Non-negative matrix factorization algorithms greatly improve topic model fits. *arXiv preprint arXiv:2105.13440*, 2021.

Kushal K Dey, Chiaowen Joyce Hsiao, and Matthew Stephens. Visualizing the structure of rna-seq expression data using grade of membership models. *PLoS genetics*, 13(3):e1006599, 2017.

Andrew Gelman. Exploratory data analysis for complex models. *Journal of Computational and Graphical Statistics*, 13(4):755–779, 2004.

Andrew Gelman and Cosma Rohilla Shalizi. Philosophy and the practice of bayesian statistics. *British Journal of Mathematical and Statistical Psychology*, 66(1):8–38, 2013.

Carmen Bravo González-Blas, Liesbeth Minnoye, Dafni Papasokrati, Sara Aibar, Gert Hulselmans, Valerie Christiaens, Kristofer Davie, Jasper Wouters, and Stein Aerts. cistopic: cis-regulatory topic modeling on single-cell atac-seq data. *Nature methods*, 16(5):397–400, 2019.

Susan P Holmes and Wolfgang Huber. *Modern statistics for modern biology*. Cambridge University Press, 2018.

Pratheepa Jeganathan and Susan P Holmes. A statistical perspective on the challenges in molecular microbial biology. *Journal of Agricultural, Biological and Environmental Statistics*, 26(2):131–160, 2021.

- Robert E Kass and Adrian E Raftery. Bayes factors. *Journal of the american statistical association*, 90(430):773–795, 1995.
- Márcio FA Leite and Eiko E Kuramae. You must choose, but choose wisely: model-based approaches for microbial community analysis. *Soil Biology and Biochemistry*, 151:108042, 2020.
- Marina Meilă. Comparing clusterings—an information based distance. *Journal of multivariate analysis*, 98(5):873–895, 2007.
- Gabriel Peyré, Marco Cuturi, et al. Computational optimal transport: With applications to data science. *Foundations and Trends® in Machine Learning*, 11(5-6):355–607, 2019.
- Katherine S Pollard and Mark J Van Der Laan. Cluster analysis of genomic data. In *Bioinformatics and Computational Biology Solutions Using R and Bioconductor*, pages 209–228. Springer, 2005.
- Gabriel K Reder, Adamo Young, Jaan Altosaar, Jakub Rajniak, Noémie Elhadad, Michael Fischbach, and Susan P Holmes. Supervised topic modeling for predicting molecular substructure from mass spectrometry. *F1000Research*, 10(403):403, 2021.
- Kris Sankaran and Susan P Holmes. Latent variable modeling for the microbiome. *Biostatistics*, 20(4):599–614, 2019.
- John W Tukey. *Exploratory data analysis*, volume 2. Reading, Mass., 1977.
- Silke Wagner and Dorothea Wagner. *Comparing clusterings: an overview*. Universität Karlsruhe, Fakultät für Informatik Karlsruhe, 2007.
- Hanna M Wallach, Iain Murray, Ruslan Salakhutdinov, and David Mimno. Evaluation methods for topic models. In *Proceedings of the 26th annual international conference on machine learning*, pages 1105–1112, 2009.

SUPPLEMENTARY MATERIALS

1. PROPERTIES OF THE REFINEMENT SCORE

Our definition of the refinement score is

$$\begin{aligned} r(v) &:= \frac{1}{L-l} \sum_{l'=l+1}^L \sum_{v'_{l'} \in V_{l'}} w_{\text{out}}(v, v'_{l'}) w_{\text{in}}(v, v'_{l'}) \\ &= \frac{1}{L-l} \sum_{l'=l+1}^L \sum_{v'_{l'} \in V_{l'}} \frac{w(v, v'_{l'})^2}{(\sum_{u \in V_l} w(u, v'_{l'}))(\sum_{w \in V_{l'}} w(v, w))} \end{aligned}$$

where V_l is the set of all nodes in level l .

Here we give proofs for the assertions about the refinement score given in the main text.

Maximizing $r(v)$

Suppose v is in level l , and suppose further that $w(v, v'_{l'}) > 0$ implies $w(u, v'_{l'}) = 0$ for any $u \in V_l \setminus \{v\}$. This means that every node in level l' has only one parent in level l . In that case, $\sum_{u \in V_l} w(u, v'_{l'}) = w(v, v'_{l'})$, and we can write the inner sum in the definition of $r(v)$ as

$$\begin{aligned} \sum_{v'_{l'} \in V_{l'}} \frac{w(v, v'_{l'})^2}{(\sum_{u \in V_l} w(u, v'_{l'}))(\sum_{w \in V_{l'}} w(v, w))} &= \frac{1}{\sum_{w \in V_{l'}} w(v, w)} \sum_{v'_{l'} \in V_{l'}} \frac{w(v, v'_{l'})^2}{\sum_{u \in V_l} w(u, v'_{l'})} \\ &= \frac{1}{\sum_{w \in V_{l'}} w(v, w)} \sum_{v'_{l'} \in V_{l'}} w(v, v'_{l'}) = 1 \end{aligned}$$

Then the overall value for the refinement score is

$$\begin{aligned} r(v) &= \frac{1}{L-l} \sum_{l'=l+1}^L \sum_{v'_{l'} \in V_{l'}} \frac{w(v, v'_{l'})^2}{(\sum_{u \in V_l} w(u, v'_{l'}))(\sum_{w \in V_{l'}} w(v, w))} \\ &= \frac{1}{L-l} \sum_{l'=l+1}^L 1 = 1 \end{aligned}$$

This is the largest $r(v)$ can be, as can be seen by noting that if $w(u, v'_{l'}) > 0$ for some

$u \in V_l \setminus \{v\}$, we will have

$$\begin{aligned} \sum_{v' \in V_{l'}} \frac{w(v, v'_{l'})^2}{(\sum_{u \in V_l} w(u, v'_{l'}))(\sum_{w \in V_{l'}} w(v, w))} &= \frac{1}{\sum_{w \in V_{l'}} w(v, w)} \sum_{v' \in V_{l'}} \frac{w(v, v'_{l'})^2}{\sum_{u \in V_l} w(u, v'_{l'})} \\ &< \frac{1}{\sum_{w \in V_{l'}} w(v, w)} \sum_{v' \in V_{l'}} \frac{w(v, v'_{l'})^2}{w(v, v'_{l'})} \\ &= \frac{1}{\sum_{w \in V_{l'}} w(v, w)} \sum_{v' \in V_{l'}} w(v, v'_{l'}) = 1 \end{aligned}$$

Therefore, a node will have a refinement score of 1 if and only if every node in level $l' > l$ has only one parent in level l .

Note that if all the refinement scores are 1, then each node will have only one parent in the previous level, and the graph visualized will be a tree. However, the parent-child relationships ($l' - l = 1$) do not have to be consistent with the ancestor-descendant ($l' - l > 1$) relationships for all of the refinement scores to be 1.

Minimizing $r(v)$

Suppose we want to minimize $r(v)$ for a node v in level l . We can write the inner sum in the definition of $r(v)$ as

$$\begin{aligned} \frac{1}{\sum_{w \in V_{l'}} w(v, w)} \sum_{v' \in V_{l'}} \frac{w(v, v'_{l'})^2}{\sum_{u \in V_l} w(u, v'_{l'})} \\ = \frac{1}{\sum_{w \in V_{l'}} w(v, w)} \sum_{v' \in V_{l'}} \frac{w(v, v'_{l'})}{1 + \sum_{u \in V_l \setminus \{v\}} w(u, v'_{l'}) / w(v, v'_{l'})} \end{aligned}$$

Supposing that the weights $w(v, w)$, $w \in V_{l'}$ are fixed, the quantity above goes to zero when for each $v'_{l'}$ s.t. $w(v, v'_{l'}) > 0$, $w(u, v'_{l'}) \rightarrow \infty$ for some $u \in V_l \setminus \{v\}$. The refinement score $r(v)$ is an average over these values, and so the refinement score will also go to zero. Therefore, for $r(v)$ to be small, all the descendants of v need to primarily descend from some other node in the same level as v .

Refinement scores when all the weights are equal

One of the “edge” cases we are particularly interested in is one in which all the weights are equal.

This is our intuition about what will happen if the clusters in the different levels don’t correspond to each other at all.

If all the edges are equal, no matter what l is, we will have $w_{\text{in}}(v, v'_{l'}) = \frac{1}{|V|}$, and so the expression for the refinement score simplifies to

$$\begin{aligned} r(v) &= \frac{1}{L-l} \sum_{l'=l+1}^L \sum_{v'_{l'} \in V_{l'}} w_{\text{out}}(v, v'_{l'}) w_{\text{in}}(v, v'_{l'}) \\ &= \frac{1}{|V|(L-l)} \sum_{l'=l+1}^L \sum_{v'_{l'} \in V_{l'}} w_{\text{out}}(v, v'_{l'}) = \frac{1}{|V|} \end{aligned}$$

Overall, these results show us how the refinement scores work, and give us some insight into how the weights that we don’t visualize enter into the refinement score calculations. For example, if we had an alignment graph for which all the weights between subsequent levels were equal, we could still have a node with a relatively high refinement score if the weights that we didn’t see satisfied the criteria for maximizing the refinement score (each node in a later level has only one ancestor in the level of the node we are interested in). On the other hand, the alignment graph could look like a tree when we just look at the weights between subsequent levels, but if the weights in the levels we don’t see are either all equal or such that the node we are interested in doesn’t have descendants in the later levels, its refinement score could be very small.

2. SUPPLEMENTARY FIGURES

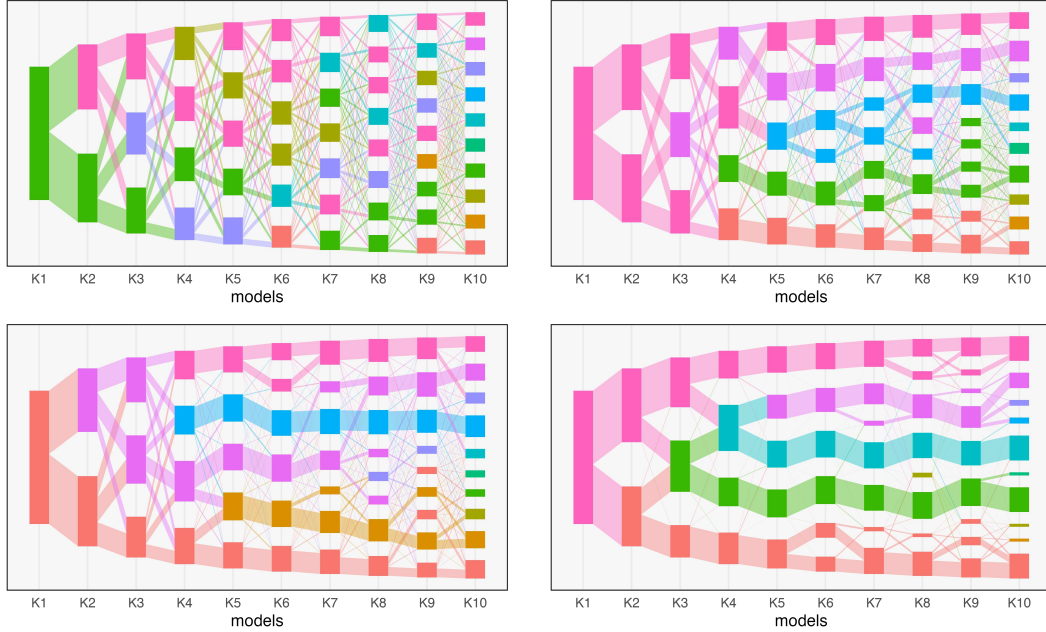


Fig. 1: Flows for LDA with background variation at levels $\alpha \in \{0, 0.4, 0.6, 1\}$. A more definitive topic structure emerges for larger α , with less exchange between neighboring branches.

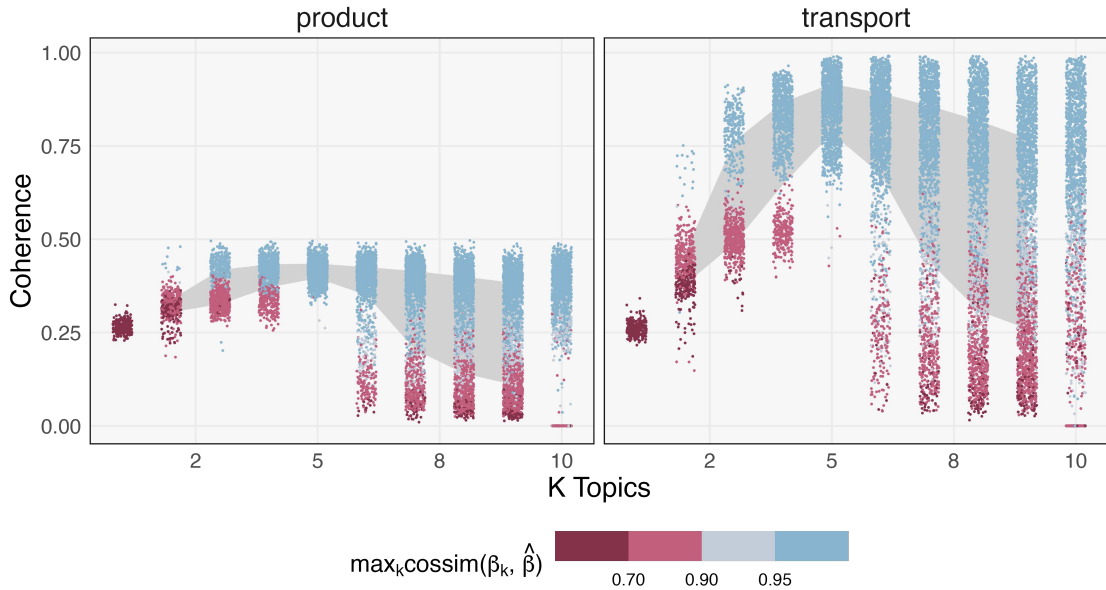


Fig. 2: Coherence scores for topics estimated in a true LDA model with $K = 5$. As with the refinement measure discussed in the main text, coherence highlights the true latent dimensionality.

3. STRAIN SWITCHING ACROSS S

In this appendix, we extend the discussion of strain switching. We provide details of the perturbation mechanism (Algorithm 1) and investigate the sensitivity of topic alignment across a wider range of S . We simulate strain-switching data for $S \in \{10, 30, \dots, 230\}$. For each choice of S , we generate 50 datasets and align topic models across a range $K = 2, \dots, 10$ of topics.

To gauge sensitivity to perturbed topics, we measure cosine similarities across simulation replicates. If strain switching cannot be detected, then we expect $\xi_{1k}^m \approx \xi_{2k}^m$ and $\xi_{3k}^m \approx \xi_{4k}^m$ for all k, m — the estimated topics will lack specificity for any member of the equivalent pairs. Figure 3 shows the estimation specificity, $\frac{1}{K} \sum_{k=1}^m |\xi_{1k}^m - \xi_{2k}^m| + |\xi_{3k}^m - \xi_{4k}^m|$ for each of the 50 replicates for each S . This statistic quantifies the difference between rows 1-2 and 3-4 visible in the heatmap of topic similarities, but across all simulation replicates.

As expected, larger perturbations are more easily detected. For models with $K \leq 5$, there is a small increase in estimation specificity as S increases; strain switching might have a small effect on the dominant signatures in the data. For $K > 5$, the specificity as a function of S steepens —

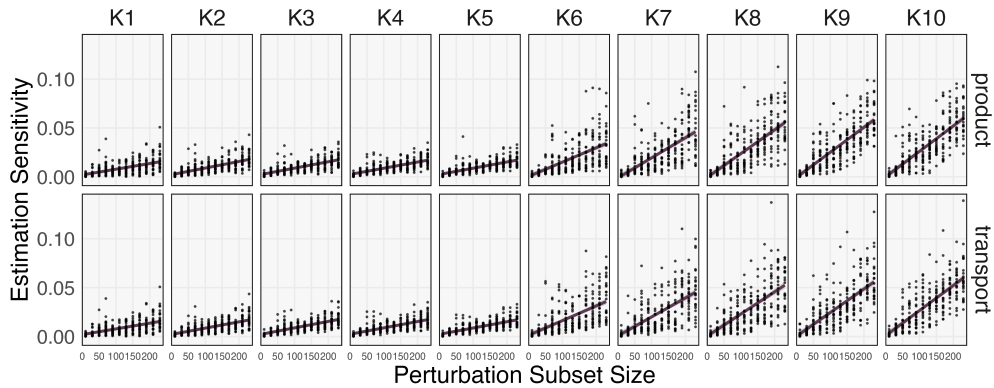


Fig. 3: The ability of models to detect strain switching as a function of K and S . Model resolution increases across panels moving from left to right. Within each panel, the size of the number of swapped species S is plotted against the estimation sensitivities defined in the main text. The larger the subset S , the higher the sensitivity. Further, high-resolution models can more easily distinguish perturbed topics, as indicated by the steeper slopes for panels on the right.

more highly resolved topics can more easily distinguish between perturbed topics.

Data: Topics β_k , subset size S to perturb, \tilde{K} of the topics to perturb, number of perturbations R .

```

for  $k \leq \tilde{K}$  do
    Sample  $S$  coordinates to perturb, and define a mapping  $\pi$  such that  $\pi(s)$  provides
    the  $s^{th}$  perturbed index.

    for  $r \leq R$  do
        For the subset  $S$ , draw  $\nu_k^r \sim \text{Dir}(\lambda_S \mathbf{1}_{|S|})$ 
        Renormalize  $\nu_k^r := \frac{\|\beta_k[S]\|_1}{\|\nu_r\|_1} \nu_r$ 
        Perturb  $\beta_k$  at coordinates specified by  $S$ ,
        
$$\tilde{\beta}_{kd}^r := \begin{cases} \beta_{kd} & \text{if } d \notin S \\ \nu_{k\pi(s)}^r & \text{otherwise.} \end{cases}$$

    end
end

```

Algorithm 1: Strategy for generating perturbed topics.